

# Microthermoforming of microfluidic substrates by soft lithography ( $\mu$ TSL): optimization using design of experiments

M Focke<sup>1</sup>, D Kosse<sup>2</sup>, D Al-Bamerni<sup>1</sup>, S Lutz<sup>2</sup>, C Müller<sup>3</sup>, H Reinecke<sup>2,3</sup>,  
R Zengerle<sup>1,2,4</sup> and F von Stetten<sup>1,2</sup>

<sup>1</sup> Laboratory for MEMS Applications, Department of Microsystems Engineering—IMTEK, University of Freiburg, Georges-Koehler-Allee 106, 79110 Freiburg, Germany

<sup>2</sup> HSG-IMIT, Wilhelm-Schickard-Straße 10, D-78052 Villingen-Schwenningen, Germany

<sup>3</sup> Laboratory for Process Technology, Department of Microsystems Engineering—IMTEK, University of Freiburg, Georges-Koehler-Allee 103, 79110 Freiburg, Germany

<sup>4</sup> BIOS Centre for Biological Signalling Studies, University of Freiburg, Germany

E-mail: [vstetten@imtek.de](mailto:vstetten@imtek.de)

Received 23 May 2011, in final form 10 August 2011

Published 3 October 2011

Online at [stacks.iop.org/JMM/21/115002](http://stacks.iop.org/JMM/21/115002)

## Abstract

We present a detailed analysis of microthermoforming by soft lithography ( $\mu$ TSL) for replication of foil-based microfluidic substrates. The process was systematically optimized by design of experiments (DOE) enabling fabrication of defect-free lab-on-a-chip devices. After the assessment of typical error patterns we optimized the process toward the minimum deviation between mold and thermoformed foil substrates. The following process parameters have most significant impact on the dimensional responses ( $p < 0.05$ ): critical temperature before start of evacuation, molding temperature, pressure of pre-stretching and duration of pre-stretching as well as duration of molding pressure. The most relevant parameter is molding temperature with  $>40\%$  relative impact. The DOE results in an empirical process model with a maximum deviation between the prediction and experimental proof of 2% for the optimum parameter set. Finally, process optimization is validated by the fabrication and testing of a microfluidic structure for blood plasma separation from human whole blood. The optimized process enabled metering of a nominal volume of  $4.0 \mu\text{l}$  of blood plasma with an accuracy deviation of 3% and a metering precision of  $\pm 7.0\%$ . The  $\mu$ TSL process takes about 30 min and easily enables the replication of  $300 \mu\text{m}$  wide microchannels having vertical sidewalls without any draft angles in a well-controllable way. It proves to be suitable for multiple applications in the field of microfluidic devices.

 Online supplementary data available from [stacks.iop.org/JMM/21/115002/mmedia](http://stacks.iop.org/JMM/21/115002/mmedia)

(Some figures in this article are in colour only in the electronic version)

## 1. Introduction

The process of microthermoforming by soft lithography ( $\mu$ TSL) is analyzed and optimized by design of experiments (DOE). The particular focus of this work is oriented toward the defect-free replication of microfluidic substrates.

The fabrication of microfluidic devices made-up of polymers is already well established [1], especially

by employing elastic materials like polydimethylsiloxane (PDMS) [2] or thermoplastic materials [3]. The latter are frequently processed by either laser technologies [4], hot embossing [5] or injection molding [6] which allows high throughputs and thus cost-efficient mass production. In contrast, the technology of microthermoforming is adopted from its macroscale counterpart. Industrial thermoforming [7] produces for instance millions of disposable blister

packages for food or pharmaceutical products every day [8, 9]. We expect that microfabrication and particularly microfluidics can profit considerably from the sector of industrial packaging [10], with microthermoforming being a prime example. Microfluidic lab-on-a-chip devices [11] take significant advantage when fabricated as disposable foil-based substrates. Such disposables only require a minimum of material and allow efficient thermocycling due to their low thickness as required in nucleic acid analysis by polymerase chain reaction (PCR) [12, 13].

The process of microthermoforming in principle is simple: a thermoplastic foil is first heated beyond its glass transition temperature. Then a pressure difference on either side of the foil is applied which forms the soft foil onto a mold to replicate its topography [14] resulting in substrates with three-dimensional geometries having thin walls [7, 10, 15].

However, microfluidic devices make certain demands of the replication process. First of all, process robustness must be ensured in order to provide sufficient replication accuracy. Secondly, high shape fidelities with typical tolerance bands in the micron-scale are required. Accurate molding of sharp edges plays an important role when defined conditions for liquid handling are required, for example, in metering or pinning of discrete liquid volumes or droplet cutting in continuous segmented flow. Thirdly, process applicability is greatly expanded when complex structures are feasible, for example, high aspect ratios or very shallow geometries in close proximity to very deep ones.

The principles of microthermoforming were initially introduced by Truckenmüller *et al* [16]. Shortly after, Chang *et al* published a similar process which they named gas pressurized hot embossing [17]. So far, a number of biomedical microdevices have been realized [18], e.g., in the field of tissue engineering [19–21] and nucleic acid analysis [22–24]. However, a systematic analysis of the process has not been presented so far. A comprehensive understanding of microthermoforming, though, is required to further exploit its potential for a low-cost and precise mass production of microparts. Additionally, in the early years all authors assumed that processes of microthermoforming would be limited to rounded structures with small aspect ratios and low-dimensional precision [3, 15, 16, 25, 26]. In contrast to that, we demonstrate here that the  $\mu$ TSL approach enables precise shaping of microstructures with defined geometries as well as forming of sharp features such as edges or corners. Other than conventional microthermoforming processes, positive molds made from flexible PDMS are applied in our  $\mu$ TSL approach. This concept is transferred from the well-established technique of replica molding by  $\mu$ TSL techniques [27, 28].

The method is first of all meant for rapid prototyping of foil-based microfluidic devices before up-scaling of chip fabrication. The  $\mu$ TSL technique is advantageous in several ways: the construction of molds is facilitated because draft angles or bevels are not required due to the flexibility of the foil substrate and the PDMS mold enabling simple demolding. Additionally, the process requires only one mold, unlike conventional hot embossing, micro-imprinting or injection

molding which need two mold halves [29] or at least an elastomeric counterplate [30].

After the characterization of typical error patterns in microthermoforming and their possible reasons, a tailored master mold is introduced containing certain critical microfluidic geometries. These are replicated in varying experimental runs in the course of a systematic design of experiment. The relative deviations of the molded geometries from the master mold are selected as suitable response values. Their analysis is based on a central composite design to set up an empirical model of the response surface [31]. This allows the identification of all factor interactions and the definition of an optimum-operating regime for best achievable response values (i.e. the lowest deviation from master mold). The improvements of the process optimization are finally validated by a microfluidic structure for separation and metering of blood plasma from human whole blood on a centrifugal microfluidic platform.

## 2. Materials and methods

This section describes the fabrication process for molds and the required machine equipment. The principles of the  $\mu$ TSL process are introduced together with all relevant process parameters. Finally, the DOE approach is briefly outlined.

### 2.1. Molds

The master mold is micromilled in a plate of polymethylmethacrylate [32] and subsequently cast with PDMS (Elastosil RT 607, Wacker Chemie AG, Germany). The uncured PDMS is first evacuated at approximately 2 kPa (absolute pressure) in order to remove air bubbles in the pre-polymer. Subsequently, the PDMS is cured at 90 °C at atmospheric pressure for 20 min. Before using a PDMS mold, it must be heat-treated for 1 h at 200 °C and 0.5 kPa (absolute pressure) in order to assure defined conditioning. Heat treatment causes monomers and moisture in the PDMS matrix to outgas. As a consequence, a PDMS mold can shrink up to 2.5%. The conditioned PDMS molds finally serve as positive molds for microthermoforming.

### 2.2. Thermoforming machine

An upgraded hot embossing machine (HEX 01, Jenoptik AG, Germany) is employed for microthermoforming. The modifications comprise an additional nitrogen feed-in from the upper cross-head as well as the replacement of the standard embossing chuck [33] by a custom made aluminum mold support (figure 1). The nitrogen feed-in features a valve that allows precise pressure control in the process chamber.

### 2.3. The microthermoforming process

A thermoplastic foil is placed on top of the mold. The aluminum mold support and the upper clamp tool are heated to the temperature  $T_e$  at which the process chamber is evacuated to a vacuum pressure  $p_{vac}$  and is subsequently closed (figure 2). The temperature  $T_e$  should be as close to

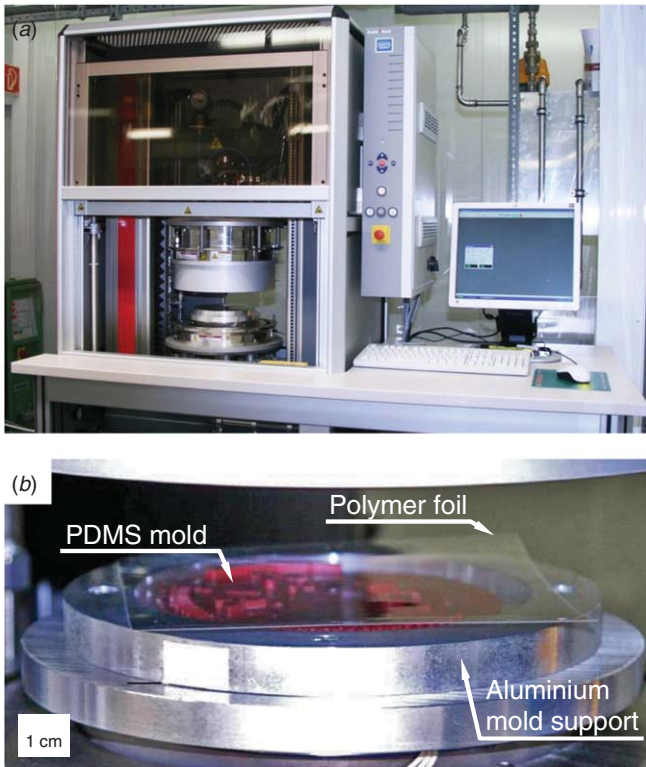


**Figure 1.** Hot embossing machine upgraded for microthermoforming. (a) Machine in full size and on standby. (b) Close-up of open process chamber with mold and polymer foil.

the molding temperature  $T_m$  as possible so that heating is supported by convection, which is no longer possible in the evacuated state. The foil is firmly clamped by closing the clamp holder and the mold support with a force of 15 kN. This separates the process chamber into a space above and below the foil. The assembly is further heated beyond the glass transition temperature  $T_g$  of the polymer foil up to the molding temperature  $T_m$ .

At  $T_m$ , a pressure  $p_1$  is applied by pressurizing the space above the foil. This leads to pre-stretching of the foil and a first soft contact of foil and mold resulting in improved heat transfer due to direct heat conduction. After a holding time  $t_1$ , the pressure is increased to  $p_2$  and held again for a time  $t_2$  in order to allow precise molding. Afterward, the machine is cooled and vented to atmospheric pressure. Finally, the foil is detached from the mold.

In this study, the initial vacuum pressure is kept constant at 0.1 kPa (absolute pressure). We further apply only one type of foil material for simplification: cyclic olefin polymer (COP, ZF14, Zeon Chemicals L. P., USA) with a thickness of 188  $\mu\text{m}$  and a glass transition temperature  $T_g$  of 135  $^\circ\text{C}$  (FP 90 DTA, Mettler Toledo GmbH, Germany). Its properties are beneficial for various microfluidic applications due to its high thermal and mechanical stability, high transparency and biological inertness [34, 35]. Nevertheless, other materials such as polystyrene or polyamide are also suitable for microthermoforming [19].

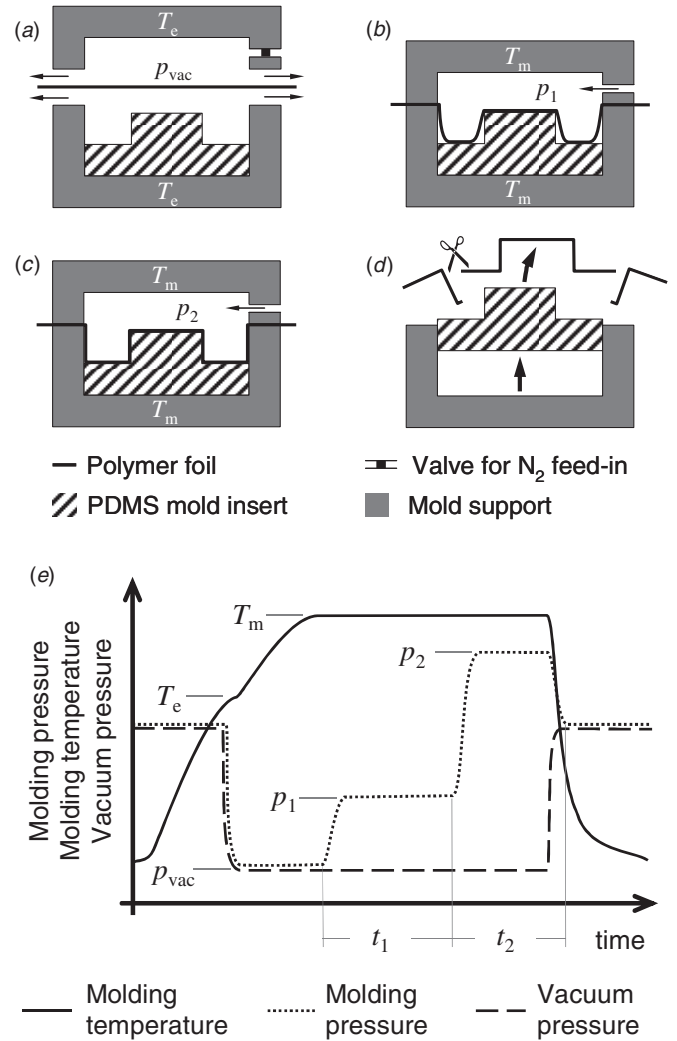


**Figure 2.** Process flow of microthermoforming. (a) Assembly in the process chamber, evacuation and heating. (b) Foil pre-stretching by pressurizing the space above the foil at pressure  $p_1$  and molding temperature  $T_m$ . (c) Molding at pressure  $p_2$ . (d) Detachment and trimming after cooling and venting. (e) Schematic process chart.

#### 2.4. Design of experiments

The process is analyzed and finally optimized by a systematic DOE. The parameter regime near the optimum is determined by the input factors  $x_i$  ( $i = 1, 2, \dots, k$ ) and the estimate response vector  $\hat{y}$ . The hypercubic curvature of the response surface can be described by a model of second order with a set of coefficients  $\vec{a}$  [36], here exemplary with the consideration of two-factor interactions  $x_i x_j$  ( $i < j \leq k$ ):

$$\hat{y} = \vec{a}_0 + \sum_{i=1}^k (\vec{a}_i x_i) + \sum_{i=1}^k \vec{a}_{ii} x_i^2 + \sum_{i=1}^k \sum_{j=1, j \neq i}^k \vec{a}_{ij} x_i x_j. \quad (1)$$

Systematic experiments and least-squares regression methodologies allow us to estimate the coefficients  $\vec{a}$  and to set up an empirical model. Finally, it is possible to compute a combination of input factors that generates optimal responses. Since this is a multi-response problem, a compromise must be found that not only optimizes one but all desired responses at the

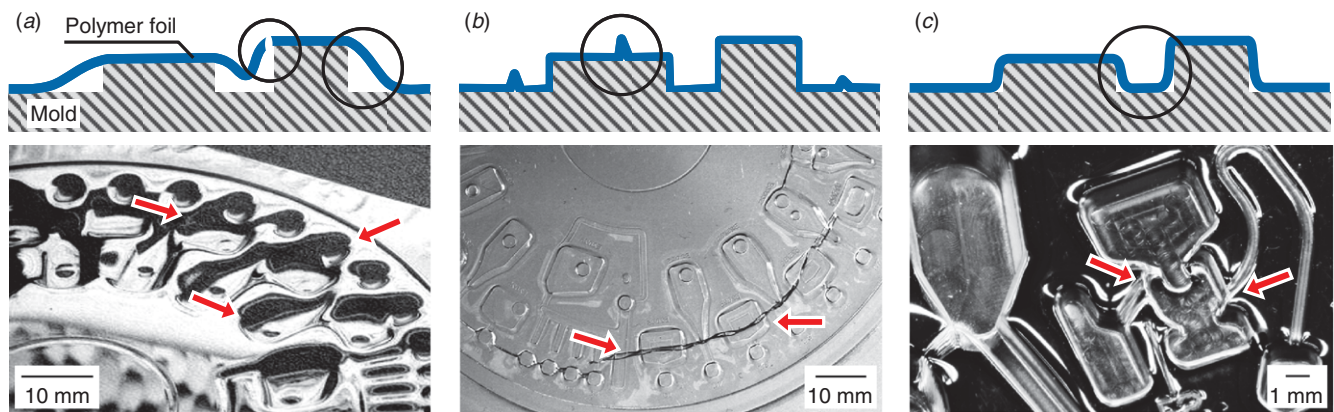


**Figure 3.** Main error patterns in microthermoforming. (a) Holes lead to neutralization of the pressure difference and thus mismatches. (b) Wrinkles are caused by insufficient evacuation. (c) Rounded, non-sharp edges occur due to suboptimal factor combinations near the optimal operating regime.

same time [37]. One preferred solution to this problem is the use of desirability functions [38], which is discussed later in more detail.

The experimental design is separated into two phases. The first phase is a screening design to identify significant as well as insignificant factors for the process responses by a two-level fractional factorial design. The aim of the first phase is to reduce the total amount of required runs and to find a sufficient center point for the following second phase. The second phase is a response surface design to find operating conditions for optimal responses with a two-level full factorial design. For both phases we employed central composite designs.

The software JMP<sup>®</sup> 8.0 (SAS Institute Inc., Cary, USA) was used for the analysis and optimization of all data obtained from the experiments. Dimensional responses are either measured with a calibrated reflected-light microscope (Axiovert 25 HD, Carl Zeiss AG, Germany) or with a digital video-measuring machine (Visio 300 DCC, Tesa Technology SA, Switzerland). The application of the respective instrument depends on the size and accessibility of the measurement location. Both instruments have a measurement uncertainty of  $\pm 1 \mu\text{m}$ .

### 3. Results and discussion

In the following section typical error patterns are characterized and the types of responses that are used for the experimental design are discussed. Then, the master mold is described followed by the results of the DOE and further processes analysis. Finally, the quality of foil replicas fabricated with the optimum process parameters is validated by testing a microfluidic metering structure for blood plasma separation from human whole blood.

#### 3.1. Error patterns

Sufficient molding is achieved when the foil fully replicates the topography of the mold. However, three different error patterns can be distinguished when the main influential factors are not in the optimal processing range: severe mismatches

caused by rupturing of the foil, wrinkles in the molded substrate, and finally rounded, non-sharp edges.

When the thermoforming process causes rupturing of the foil, small holes are formed leading to severe mismatches with ‘tent-like’ appearance. When ‘tents’ appear in the thermoformed substrate, the polymer foil hardly replicates the shape of the mold. The foil rather spans from one mold structure to the next so that it does not touch the surface of the mold plane sufficiently (figure 3(a)). The tent error basically affects the replication of all structures of a mold. As a consequence of the generated hole in the foil the pressure difference between the space above and below the foil is equalized. Rupturing can occur when the pre-stretching pressure  $p_1$  is too high or the temperature of the foil is too low. Brittle thermoplastic materials such as COP or polycarbonate (PC) are more likely to be affected than softer and more elastic materials such as polypropylene (PP) or polyvinyl chloride (PVC). The rupture of the foil usually occurs at geometries that require a high degree of stretching, for example, structures with a high aspect ratio and large dimensions in relation to foil thickness. The obtainable aspect ratios are generally limited for both positive and negative molds by the thickness of the foil since the foil is stretched during molding [3].

Wrinkles can occur with varying sizes across the complete replicated substrate (figure 3(b)). Wrinkles indicate gas entrapments in the space below the foil during the molding phase. The gas entrapments are air pockets that collapse when the molding pressure is applied. The material surplus of the air pocket eventually leads to foldings and wrinkles. The main reason for gas entrapment is insufficient evacuation of the process chamber. This can for example occur when the evacuation temperature  $T_e$  is too high. In this case, the foil could melt onto the rim of the mold support, thus acting as a sealant and preventing sufficient evacuation of the enclosed lower space. Therefore,  $T_e$  should be below  $T_g$ . Another reason for gas entrapments can be due to outgassing of the PDMS mold when it was not sufficiently conditioned in the beginning.

The first two error patterns caused by foil rupture and gas entrapments may be overcome or circumvented by some

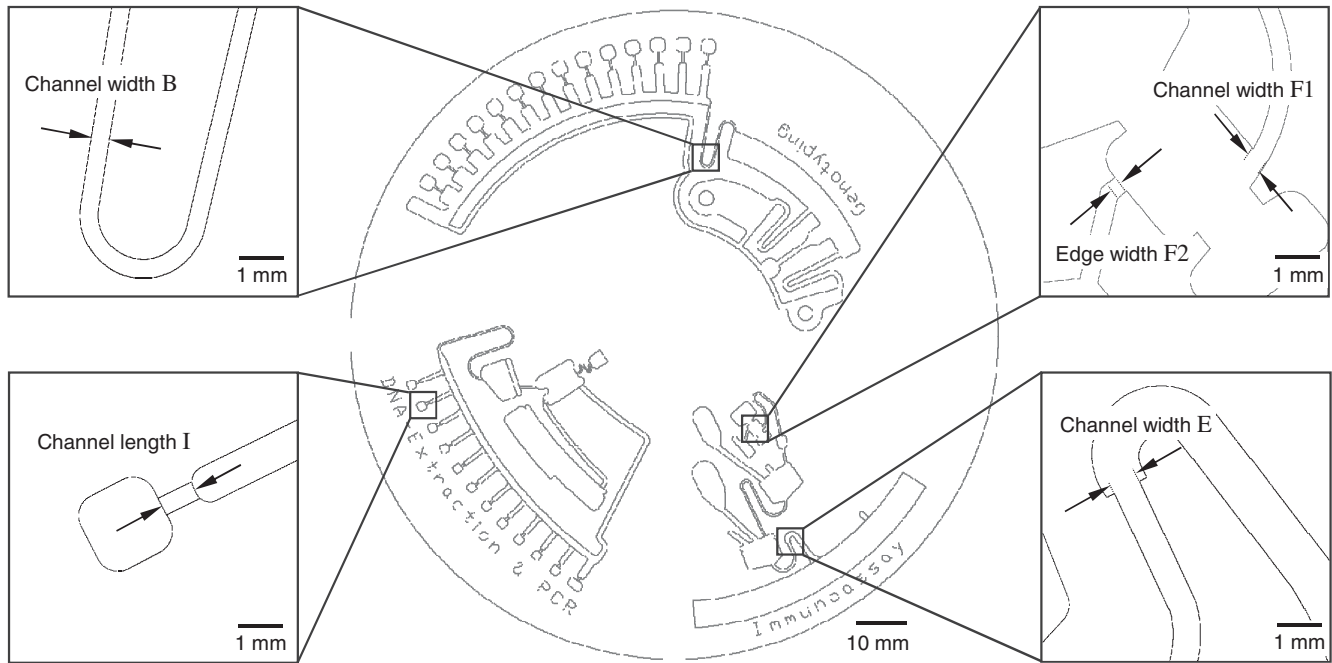


**Figure 4.** CAD layout of the master mold used for process optimization by DOE. The magnified areas show geometries that are critical for molding and frequently exhibit mismatches. The three different structures are typical for designs in centrifugal microfluidics.

basic process engineering as mentioned above. The third error of rounded, non-sharp edges still occurs when the parameters are already in the region near the optimum, but a fine-tuning has not yet been done (figure 3(c)). This error occurred at different degrees in the course of the DOE and could never be associated with a deformation of the PDMS mold. Rather, bending radius should be considered for error explanation, which typically occurs if a stiff film is bent into a corner. Sharp edges can only be formed if the polymer film softens and the material can flow around the mold contour.

### 3.2. Input factors, responses and mold design

The wall thickness of thermoformed parts is generally not uniform due to biaxial stretching of the foil during thermoforming [39]. Thermoplastic foils heated beyond  $T_g$  exhibit viscoelastic properties. That means that both plastic flow and elastic deformation of the polymeric macromolecules occur. Both depend on time and temperature as well as shear stress induced by the applied pressure difference. Thus, an adequate combination of molding temperature, molding duration and pressure must be found to provide a sufficient degree of deformation [40]. Therefore, the following five factors were selected for DOE: critical temperature before start of evacuation  $T_e$ , molding temperature  $T_m$ , pressure of pre-stretching  $p_1$ , duration of pre-stretching  $t_1$  and duration of molding  $t_2$  at full molding pressure  $p_2$  (see figure 2). Polymer foil and vacuum pressure  $p_{vac}$  were kept constant throughout all experiments. The set point of the molding pressure  $p_2$  was 310 kPa (absolute pressure) due to the limited clamp force of the hot embossing machine unit.

The quality of molding is derived from characteristic geometries in a typical microfluidic design that is incorporated

on a master mold for process optimization (figure 4). Due to our specialization on centrifugal microfluidics [41], our molds have a circular shape with a diameter of 130 mm. The master mold contains three typical microfluidic structures as often used in our lab. Among these are microfluidic structures for an immunoassay [42], nucleic acid extraction [43] and genotyping by real-time PCR [24] (it should be noted that these structures are usually not combined on one disk).

A basic, suboptimal process delivers improper molding of some critical geometries on the master mold. These critical structures for example determine the conditions of capillary priming, metering volumes or sharp edges for pinning of menisci. These critical geometries are chosen as response values for the DOE. Their nominal values are based on the micromilled master mold. Geometries B, E and F1 are channel widths of nominally 373, 599 and 430  $\mu\text{m}$ , respectively. The critical structure I has a channel length of nominally 845  $\mu\text{m}$ . Finally, F2 is an edge with a nominal width of 256  $\mu\text{m}$ . Lateral dimensions of critical geometries in each replicated foil substrate were always measured from edge to edge as indicated in figure 5. Then, the relative deviation of the foil structure from the master mold is calculated and used as response for the DOE.

In order to achieve best shape fidelity, all  $n$  geometric responses (i.e. the deviations from the master mold) must be minimized. The measured values of each response  $y_m$  ( $m = 1, 2, \dots, n$ ) and their nominal values  $y_m^*$  in the master mold deliver the relative deviation  $y'_m$  as

$$y'_m = \frac{|y_m - y_m^*|}{y_m^*}. \quad (2)$$

Additionally, the process duration is taken as a further response. It has secondary priority and allows us to select

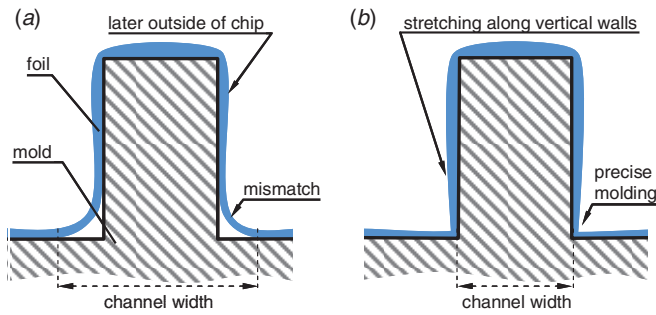


**Figure 5.** Schematic cross-section of shape fidelity in microthermoforming. (a) Improper molding with rounded, non-sharp edges (i.e. channel width too large). (b) Proper molding with ideal shape fidelity (channel width equals geometry of the mold).

**Table 1.** Input parameters and their ranges in the response surface analysis.

Factor	Lower star	Lower level	Center level	Upper level	Upper star
$T_m$ (°C)	180	190	200	210	210
$p_1$ (kPa)	12	18	24	30	36
$t_1$ (s)	500	600	700	800	900
$t_2$ (s)	50	100	150	200	250

those process parameters that enable sufficient molding in the shortest possible time.

### 3.3. Process optimization by DOE

**3.3.1. Experimental design.** In the first phase, a fractional factorial screening design with a total of 30 runs was conducted with the parameters of a basic, suboptimal process as center levels. The screening design and the respective results are found in the supplementary information (S1, tables A and B available at [stacks.iop.org/JMM/21/115002/mmedia](http://stacks.iop.org/JMM/21/115002/mmedia)). The screening results indicated that the value for temperature  $T_e$  should be at least 130 °C, which is already the upper technical limit. Evacuation at higher temperatures than 130 °C would lead to the previously described ‘sealing’ effect and would hence impair sufficient evacuation and could cause wrinkles.  $T_e$  was fixed at 130 °C and no longer examined in further analyses. From the first set of experiments an improved operating point was found that was used as a new center point for the subsequent analysis.

In the second phase, a response surface design was conducted with a full factorial design comprising 36 runs including a twelve-fold iteration of the center point (12 runs). The input parameters are selected in a narrower range than in the screening phase in order to examine the response surface more accurately (table 1). The design matrix and the results of the response surface design are found in the supplementary information (S2, table C available at [stacks.iop.org/JMM/21/115002/mmedia](http://stacks.iop.org/JMM/21/115002/mmedia)).

**3.3.2. Relevance of input factors.** The response surface design allows us to examine the effects of all input factors

and their interactions. Subsequently, the significance of the effects is estimated by a  $t$ -test. All main factors and a number of interactions were found to be significant for the process (probability of error  $p < 0.05$ ). The empirical curvature model (1) is a summation of all significant factors and factor interactions multiplied by their respective coefficients  $\vec{a}$ . The relevance (or ‘weight’) of each factor is indicated by the absolute value of its respective coefficient provided that all factors are normalized [44]. Factors and factor interactions with the largest coefficients (absolute values) contribute most to the response and hence bear highest relevance. As all geometric response values  $y'_m$  are relative deviations from the master mold, this comparison is not distorted either. The normalized input factors  $x'_i$  are determined by the range of the respective upper levels  $x_{i,max}$  and lower levels  $x_{i,min}$  as defined for the DOE:

$$x'_i = \frac{2x_i - x_{i,max} - x_{i,min}}{x_{i,max} - x_{i,min}} \quad (3)$$

Thus, the normalized input factors  $x'_i$  are coded with values between  $-1$  and  $+1$  for the lower and upper levels of the factors, respectively. Due to a circumscribed central composite design, the respective star points are ‘out of range’ with very low ( $-2$ ) or very high ( $+2$ ) values.

The empirical model (1) based on those normalized factors and geometric responses is obtained by computation of the coefficients  $\vec{a}$  using least-squares methodologies (table 2) in order to estimate the curvature of the response surface in consideration of all factor interactions. This comparison is subject to normalization and must be considered as a relative indication of factor impacts in the general process design and system performance.

Molding temperature  $T_m$  has clearly the highest impact on process outcomes as expected. When only linear and quadratic factor impacts are considered, molding temperature has 40% relative impact. Additionally, it is also involved in the remaining multi-factor interactions. The column total of 0.1 for response B means that it is relatively little affected by variations of the factors compared to the other responses. This is plausible due to the fact that B corresponds to the relative simple geometry of a microchannel with an equilateral cross-section which was already properly moldable with the basic suboptimal process before DOE. All other responses represent more critical structures that are considerably more affected by factor variations (column totals in the range of 1.0–1.9) as was also observed during DOE.

**3.3.3. The optimal operating regime.** Optimization of the empirical response surface model (1) is a multivariate problem that can be adequately addressed by the desirability function [38, 45]. Each response value  $y_m$  ( $m = 1, 2, \dots, n$ ) is transformed to a desirability value  $d_m$  with  $0 \leq d_m \leq 1$ . The overall desirability  $D$  of an optimization problem with  $n$  responses is defined as the product of all desirabilities  $d_m$  [38] (see also the supplementary information S3 available at [stacks.iop.org/JMM/21/115002/mmedia](http://stacks.iop.org/JMM/21/115002/mmedia)). This way a well-balanced set of input factors leads to a high desirability value close to 1 for the whole process.

**Table 2.** Coefficients  $\bar{a}$  of normalized factors and factor interactions ( $p < 0.05$ ).

Significant factors and factor interactions		Coefficients for geometric responses					Line total <sup>a</sup>	Relative impact
		B	E	F1	F2	I		
Linear factor impacts	$T_m$	-0.01	-0.32	-0.76	-0.39	-0.35	1.84	31.2%
	$p_1$		-0.08	-0.22	-0.13	-0.08	0.50	8.5%
	$t_1$	-0.01	-0.14	-0.25	-0.12	-0.16	0.69	11.7%
	$t_2$	-0.01	-0.04			-0.14	0.18	3.1%
Quadratic factor impacts	$T_m \cdot T_m$	0.02	0.17	0.23	0.10		0.52	8.8%
	$p_1 \cdot p_1$		0.07	0.24	0.14	0.11	0.56	9.5%
	$t_1 \cdot t_1$		0.07	0.23	0.14	0.11	0.55	9.4%
	$t_2 \cdot t_2$					0.07	0.07	1.2%
Two-factor interactions	$T_m \cdot p_1$		0.05				0.05	0.8%
	$T_m \cdot t_1$	0.01	0.13			0.12	0.27	4.5%
	$T_m \cdot t_2$	0.01	0.05			0.12	0.19	3.2%
	$p_1 \cdot t_2$		-0.02				0.02	0.3%
Three-factor interactions	$t_1 \cdot t_2$	0.01	-0.02			-0.12	0.16	2.7%
	$T_m \cdot p_1 \cdot t_2$		0.02				0.02	0.3%
	$T_m \cdot t_1 \cdot t_2$	-0.01	0.02			0.12	0.16	2.7%
	$p_1 \cdot t_1 \cdot t_2$		-0.06				0.06	1.0%
Four-factor interaction	$T_m \cdot p_1 \cdot t_1 \cdot t_2$		0.06				0.06	0.9%
Column total <sup>a</sup>		0.10	1.32	1.93	1.01	1.53	5.89	100%

<sup>a</sup> Sums of absolute values of the coefficients (rounded)

**Table 3.** Process parameters before and after optimization.

	$T_e$ (°C)	$T_m$ (°C)	$p_1$ (kPa)	$t_1$ (s)	$t_2$ (s)
Initial process before DOE	130	190	19	600	300
Optimized process after DOE	130	200	26	722	145

Each response was assigned a desirability value between 0 and 1 according to its deviation from the respective geometry in the master mold. While a deviation of 0% was coded with 1, a deviation of 10% or more from the master mold was determined to be 0 with a linear decline. Optimal process responses are obtained by the maximization of the multivariate desirability functions with parameters as found in table 3. It must be noted that the maximum temperature was determined to be 200 °C instead of the proposed 210 °C of the optimization calculation. The temperature restriction is due to our preference to delimit long-term and repeated heat exposure to certain sensitive components of the machine. The duration of the optimized process is 30.5 min which on the one hand is due to the lack of heat convection in vacuum and on the other hand determined by the duration of approximately 13 min to heat and cool the machine unit in every replication cycle.

The overall desirability of the initial process before DOE was zero (i.e. unacceptable) since some of the characteristic geometries were not sufficiently moldable. For the optimized process after DOE an overall desirability of  $D = 0.93$  was achieved which is regarded as an excellent result.

### 3.4. The verification of the response surface model

The precision of the empirical process model can be validated by comparing the predicted responses with experimental results (table 4). Although the domains of the uncertainty of the estimates are relatively large, they match very well with the practical results. The accuracy of the optimized process can be determined by comparison of the experimental results with the master mold. This provides clear evidence of high shape fidelity. The responses were retransformed to their actual geometries to illustrate the fidelity and good accordance of the empirical model with the dimensions in the optimized foils compared to the master mold.

Thermoforming results before and after process optimization are shown in figure 6. Mismatches are clearly visible particularly at the rims of those structures processed before optimization. Structures processed after optimization exhibit distinctive geometries like sharp edges and corners. In fact, all critical geometries are fully moldable. The remaining

**Table 4.** Process responses. The comparison of characteristic geometries in the master mold, in foils replicated with the initial process before DOE, and geometries of foils with the optimized process.

	Master mold	Experimental results, initial process ( $N = 5$ )	Model prediction	Experimental results, optimized process ( $N = 5$ )
Channel width B ( $\mu\text{m}$ )	$373 \pm 1$	$378 \pm 1$	$377.6 \pm 4$	$378 \pm 1$
Channel width E ( $\mu\text{m}$ )	$599 \pm 1$	$1105 \pm 3$	$595.4 \pm 35$	$618 \pm 3$
Channel width F1 ( $\mu\text{m}$ )	$430 \pm 1$	$1204 \pm 3$	$410.1 \pm 92$	$437 \pm 8$
Edge length F2 ( $\mu\text{m}$ )	$256 \pm 1$	Not feasible	$263.7 \pm 32$	$255 \pm 2$
Channel length I ( $\mu\text{m}$ )	$845 \pm 1$	Not feasible	$834.0 \pm 99$	$837 \pm 2$

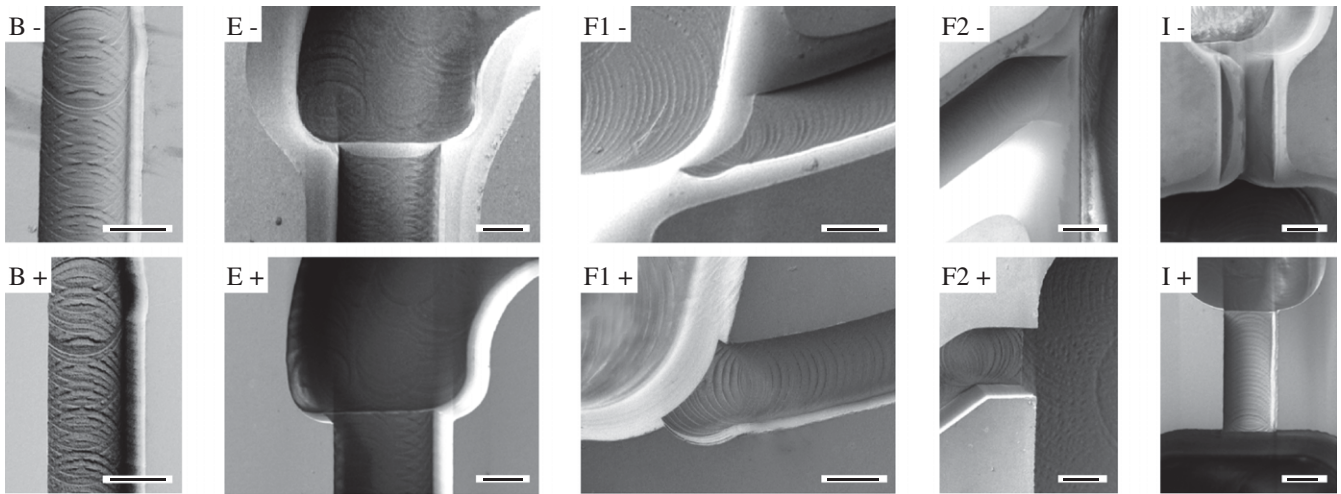


**Figure 6.** Comparison of characteristic geometries as molded before (–) and after (+) process optimization. The letter identifies the respective structure. While response *B* was not affected by the process modification, replication of all other geometries could drastically be improved. Measured geometries are schematically indicated by dashed lines. Scale bars are 200  $\mu\text{m}$ .

deviation of geometries in the master mold and foil replicates is ascribed to shrinking effects in the process of PDMS stamp preparation. The maximum deviation from the master mold is 19  $\mu\text{m}$  for geometry *E*; all others are well below 10  $\mu\text{m}$  or below 2% deviation respectively. Furthermore, replicate-to-replicate variations are also well below 10  $\mu\text{m}$ . This result is regarded as very suitable for fabrication of microfluidic devices for handling liquids in the volumetric range of microliters. Although not explicitly a subject of this study, one can assume that precise fabrication of smaller cavities and structures for handling of smaller liquid volumes would be feasible in shallower structures as well [46,47].

### 3.5. Effects of input factors

The influence of every input factor according to the empirical model of the process (see table 2) is illustrated in figure 7. Additionally, the domains of uncertainty ( $p < 0.05$ ) of the model as well as the location of the optimized point are shown. All input factors clearly show nonlinear effects. The response *B* is a relatively simple channel and almost unaffected by factor variations, as it was already moldable with the basic process. These minor effects are also found in very small uncertainties of the model for the same response. Further, some of the effects show a negative deviation response from the master mold at certain factor levels. Two cases can be discriminated: on the one hand those functions with a domain of uncertainty that also permits a positive deviation (applicable for factors  $t_1$  and  $t_2$ ) and on the other hand those functions that indicate negative deviations including the domain of uncertainty (applicable only for factor  $T_m$ ). Both cases are biased by statistical artifacts derived from the number and quality of available data points. This is particularly notable for factor  $T_m$ , which had to be varied asymmetrically due to technical limitations. The value of the upper star (+2) was set to 210  $^{\circ}\text{C}$  just as the upper level (+1) (see table 1). As a consequence, the model is not ideally adjusted but still delivers sufficient information to drastically improve the

process: the main factor to improve the thermoforming results is a temperature increase. However, it must be assured that the heat of the mold is brought into the polymer foil. This is best accomplished by a careful adjustment of the pre-stretching pressure in order to bring the foil into soft contact with the heated mold for direct heat conduction.

### 3.6. Validation of process improvement

In order to examine the benefit of the process optimization for microfluidic applications, a structure for blood separation and metered plasma extraction was fabricated with the  $\mu\text{TSL}$  process. This structure is for example required in microfluidic applications like immunoassays that demand exact volumetric metering of blood plasma in order to quantitatively determine the content of target molecules in a patient sample [42]. The structure is applied on a centrifugal microfluidic platform. First, a sample of 7  $\mu\text{l}$  of human whole blood and 7  $\mu\text{l}$  of 50 mM EDTA is inserted in the structure. Centrifugation at 50 Hz separates the blood plasma from the cellular fraction by sedimentation. The metered volume of blood plasma is determined by the filling height in the structure. Surplus liquid is centrifuged to the downstream waste reservoir. The critical geometry of the metering structure is identical to the response geometry F2 of the DOE. F2 is an edge that determines the total volume of blood plasma and blood cells for subsequent processing in the assay (figure 8). If the upper edge does not have a defined contour, the filling level in that structure is undefined and varies drastically. The actual liquid volume can be determined by a calibrated metering column which is located downstream of the capillary siphon valve. The nominal metering volume of the plasma fraction amounts to 4.0  $\mu\text{l}$ .

Based on this nominal metering volume of 4.0  $\mu\text{l}$ , the initial and suboptimal process delivered only 1.8  $\mu\text{l}$  which corresponds to 45% of the required volume (CV 14.3%,  $N = 7$  structures) because critical structures were molded insufficiently. However, the optimized process sufficiently

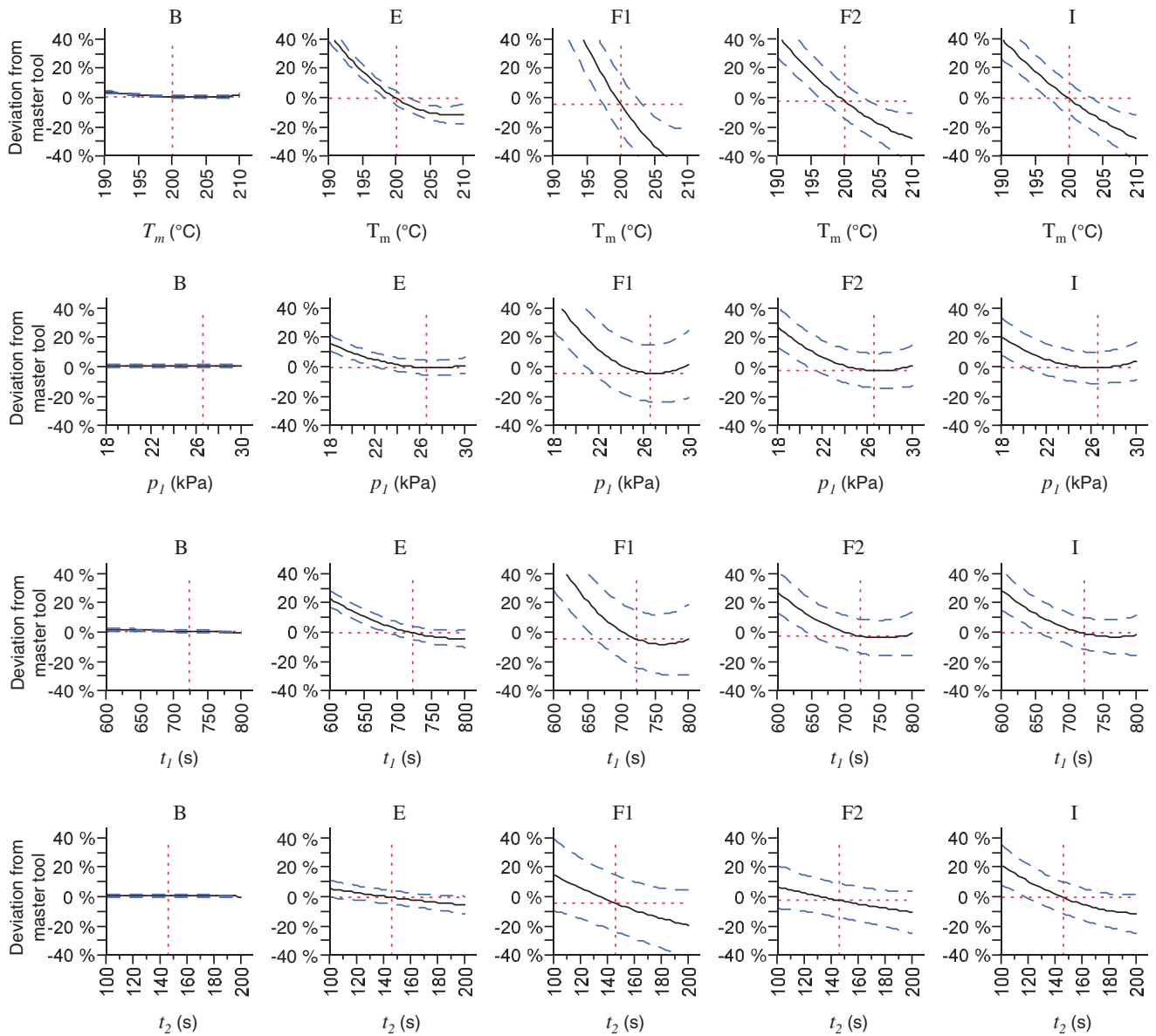


**Figure 7.** Effects of various input factors on response values. The diagrams show the predicted trend of moldability (continuous line) and its domain of uncertainty (dashed lines). The optimized operating point is found at the intersection of the dotted lines.

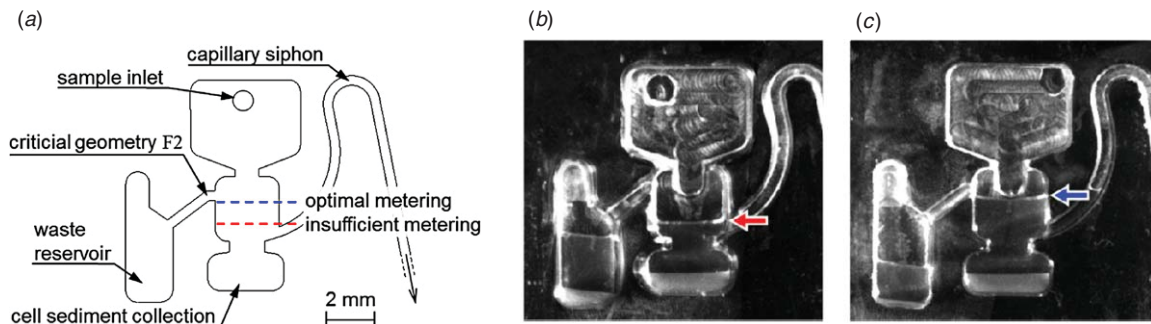


**Figure 8.** Structure for metered extraction of blood plasma. (a) Schematic structure: the total volume of blood plasma and blood cells is determined by the critical structure F2 which defines the filling level of the reservoir. Upper filling levels (b) before and (c) after process optimization. Optimal and insufficient metering corresponds to varying filling levels as indicated. The metered volume of blood plasma is removed through the siphon valve.

met the requirements of the application by metering 103% of the nominal volume (mean 4.1  $\mu\text{l}$ , CV 7.0%,  $N = 7$  structures). Both metering accuracy (i.e. mean of actual volume) and precision (i.e. coefficient of variation) could therefore be improved significantly by approximately a factor of 2 each.

#### 4. Conclusions

Microthermoforming of thin foils by  $\mu\text{TSL}$  offers significant advantages in microfluidics. A detailed analysis of the most relevant process parameters and the typical error patterns were discussed in this work. The first error pattern is caused by foil rupture that occurs when heating was insufficient or pre-stretching of the thin foil was too extreme. The holes lead to a breakdown of the pressure difference needed for sufficient replication. The second error pattern appears as wrinkles that occur due to gas entrapments from insufficient evacuation or incomplete conditioning of the PDMS mold. Finally, as a third error pattern rounded, non-sharp edges occur from sub-optimal factor combinations when the fine-tuning of the input factors is not sufficiently done.

Systematic process optimization by the DOE enabled defect-free fabrication of typical structures for microfluidic devices. High shape fidelity with replicate-to-replicate variations of characteristic geometries below 10  $\mu\text{m}$  was realized. Among the tested parameters, molding temperature has the greatest impact on moldability of critical geometries with a relative impact of more than 40%. It directly influences viscoelastic properties and thus capabilities for deformation.

Finally, the effect of process optimization was demonstrated by a considerable improvement of a microfluidic structure for the separation and metered extraction of blood plasma from human whole blood in terms of metering accuracy and precision.

Since the  $\mu\text{TSL}$  approach is for lab-scale prototyping, the process duration of roughly 30 min is acceptable and is owed to the lack of heat convection in vacuum as well as requirement of heating and cooling the complete machine for every forming cycle. In fact, cycle times for thermoforming in industrial mass production are in the range of seconds as machines are operated at constant temperatures. The significant acceleration of the  $\mu\text{TSL}$  process would be feasible with infrared radiators for heating foils faster to required temperatures. We further observed that PDMS molds show a reasonable durability as they can be applied in far more than 120 replication cycles without wear. The  $\mu\text{TSL}$  process presented here makes thermoforming of polymer foils available for research labs. This paves the way to access a highly attractive mass fabrication technology for microfluidic devices allowing us to integrate several functionalities in a cost-efficient way.

#### Acknowledgments

The research leading to these results has received funding from the European Community's Sixth Framework Programme (FP6) under contract no 37957 (project MagRSA) and funding from the German Federal Ministry of Economics and Technology via grants of the German Federation of Industrial

research Associations AIF under contract no 15838N (project BlisterLab). The authors thank Tim Hösel for contributing his expertise in DOE.

#### References

- [1] Becker H and Gartner C 2007 Polymer microfabrication technologies for microfluidic systems *Anal. Bioanal. Chem.* **390** 89–111
- [2] Sia S K and Whitesides G M 2003 Microfluidic devices fabricated in poly(dimethylsiloxane) for biological studies *Electrophoresis* **24** 3563–76
- [3] Hecke M and Schomburg W K 2004 Review on micro molding of thermoplastic polymers *J. Micromech. Microeng.* **14** R1–14
- [4] Malek C K, Robert L and Salut R 2009 Femtosecond laser machining and lamination for large-area flexible organic microfluidic chips *Eur. Phys. J.-Appl. Phys.* **46** 12503
- [5] Li J M, Liu C, Qiao H C, Zhu L Y, Chen G and Dai X D 2008 Hot embossing/bonding of a poly(ethylene terephthalate) (PET) microfluidic chip *J. Micromech. Microeng.* **18** 015008
- [6] Attia U M, Marson S and Alcock J R 2009 Micro-injection moulding of polymer microfluidic devices *Microfluidics Nanofluidics* **7** 1–28
- [7] Throne J L 1996 *Technology of Thermoforming* (Munich: Hanser)
- [8] Brody A L, Bugusu B, Han J H, Sand C K and Mchugh T H 2008 Innovative food packaging solutions *J. Food Sci.* **73** R107–16
- [9] Bauer J 2009 *Pharmaceutical Packaging Handbook* (New York: Informa Healthcare) pp 1–350
- [10] Focke M, Kosse D, Müller C, Reinecke H, Zengerle R and von Stetten F 2010 Lab-on-a-foil: microfluidics on thin and flexible films *Lab Chip* **10** 1365–86
- [11] Mark D, Haeberle S, Roth G, von Stetten F and Zengerle R 2010 Microfluidic lab-on-a-chip platforms: requirements, characteristics and applications *Chem. Soc. Rev.* **39** 1153–82
- [12] Kim Y H, Yang I, Bae Y S and Park S R 2008 Performance evaluation of thermal cyclers for PCR in a rapid cycling condition *Biotechniques* **44** 495–505
- [13] Lin Y C, Yang C C and Huang M Y 2000 Simulation and experimental validation of micro polymerase chain reaction chips *Sensors Actuators B* **71** 127–33
- [14] Illig A 2001 *Thermoforming—A Practical Guide* (Munich: Hanser)
- [15] Worgull M 2009 *Hot Embossing—Theory and Technology of Microreplication* (Burlington, MA: William Andrew)
- [16] Truckenmüller R, Rummel Z, Schaller T and Schomburg K 2002 Low-cost thermoforming of micro fluidic analysis chips *J. Micromech. Microeng.* **12** 375–9
- [17] Chang J H and Yang S Y 2003 Gas pressurized hot embossing for transcription of micro-features *Microsyst. Technol.-Micro-Nanosyst.-Inf. Storage Process. Syst.* **10** 76–80
- [18] Truckenmüller R, Giselbrecht S, Rivron N, Gottwald E, Saile V, van den Berg A, Wessling M and van Blitterswijk C 2011 Thermoforming of film-based biomedical microdevices *Adv. Mater.* **23** 1311–29
- [19] Truckenmüller R et al 2008 Flexible fluidic microchips based on thermoformed and locally modified thin polymer films *Lab Chip* **8** 1570–9
- [20] Giselbrecht S, Gietzelt T, Gottwald E, Guber A E, Trautmann C, Truckenmüller R and Weibezahn K F 2004 Microthermoforming as a novel technique for manufacturing scaffolds in tissue engineering (CellChips) *IEE Proc. Nanobiotechnol.* **151** 151–7
- [21] Giselbrecht S, Gietzelt T, Gottwald E, Trautmann C, Truckenmüller R, Weibezahn K F and Welle A 2006 3D

- tissue culture substrates produced by microthermoforming of pre-processed polymer films *Biomed. Microdevices* **8** 191–9
- [22] Focke M et al 2010 Microstructuring of polymer films for highly sensitive genotyping by real-time PCR on a centrifugal microfluidic platform *Lab Chip* **10** 2519–26
- [23] Lutz S et al 2009 Microfluidic lab-on-a-foil for nucleic acid analysis based on isothermal recombinase polymerase amplification of DNA *Lab Chip* **10** 887–93
- [24] Focke M, Stumpf F, Roth G, Zengerle R and von Stetten F 2010 Centrifugal microfluidic system for primary amplification and secondary real-time PCR *Lab Chip* **10** 3210–2
- [25] Truckenmüller R and Giselsbrecht S 2004 Microthermoforming of flexible, not-buried hollow microstructures for chip-based life sciences applications *IEE Proc. Nanobiotechnol.* **151** 163–6
- [26] Becker H and Gartner C 2007 Polymer microfabrication technologies for microfluidic systems *Anal. Bioanal. Chem.* **390** 89–111
- [27] Rogers J A and Nuzzo R G 2005 Recent progress in soft lithography *Mater. Today* **8** 50–6
- [28] Xia Y N and Whitesides G M 1998 Soft lithography *Angew. Chem.-Int. Edn* **37** 551–75
- [29] Disch A, Reinecke H and Mueller C 2007 Low cost production of disposable microfluidics by blister packaging technology *Proc. IEEE EMBS* pp 6322–5
- [30] Tan L, Kong Y P, Bao L R, Huang X D, Guo L J, Pang S W and Yee A F 2003 Imprinting polymer film on patterned substrates *J. Vac. Sci. Technol. B* **21** 2742–8
- [31] Tye H 2004 Application of statistical 'design of experiments' methods in drug discovery *Drug Discov. Today* **9** 485–91
- [32] Bundgaard F, Perozziello G and Geschke O 2006 Rapid prototyping tools and methods for all-Topas (R) cyclic olefin copolymer fluidic microsystems *Proc. Inst. Mech. Eng. C* **220** 1625–32
- [33] Becker H and Gartner C 2007 Polymer microfabrication technologies for microfluidic systems *Anal. Bioanal. Chem.* **390** 89–111
- [34] Shin J Y, Park J Y, Liu C Y, He J S and Kim S C 2005 Chemical structure and physical properties of cyclic olefin copolymers *IUPAC Technical Report, Pure Appl. Chem.* **77** 801–14
- [35] Niles W D and Coassin P J 2008 Cyclic olefin polymers: Innovative materials for high-density multiwell plates *Assay Drug Dev. Technol.* **6** 577–90
- [36] Myers R H, Khuri A I and Carter W H 1989 Response-surface methodology—1966–88 *Technometrics* **31** 137–57
- [37] Hendriks M M W B, Deboer J H, Smilde A K and Doornbos D A 1992 Multicriteria decision-making *Chemometr. Intell. Lab. Syst.* **16** 175–91
- [38] Harrington E C 1965 The desirability function *Ind. Qual. Control* **21** 494–8
- [39] Schmidt L R and Carley J F 1975 Biaxial stretching of heat-softened plastic sheets—experiments and results *Polym. Eng. Sci.* **15** 51–62
- [40] Throne J L 1991 New concepts in thermoforming *Polym.-Plast. Technol. Eng.* **30** 761–808
- [41] Ducree J, Haerberle S, Lutz S, Pausch S, von Stetten F and Zengerle R 2007 The centrifugal microfluidic bio-disk platform *J. Micromech. Microeng.* **17** 103–15
- [42] Lutz S, Lang P, Malki I, Mark D, Ducree J, Zengerle R and von Stetten F 2008 Lab-on-a-chip cartridge for processing of immunoassays with integrated sample preparation *Proc. 12th Int. Conf. on Miniaturized Systems for Chemistry and Life Sciences* pp 1759–61
- [43] Mark D, Haerberle S, Lutz S, Zengerle R and von Stetten F 2009 Vacuum supported liquid waste handling for DNA extraction on centrifugally operated lab-on-a-chip systems *Proc. 15th IEEE Int. Conf. on Solid-State Sensors, Actuators and Microsystems* pp 1230–3
- [44] Held J, Gaspar J, Ruther P, Hagner M, Cismak A, Heilmann A and Paul O 2010 Design of experiment characterization of microneedle fabrication processes based on dry silicon etching *J. Micromech. Microeng.* **20** 025024
- [45] Derringer G and Suich R 1980 Simultaneous optimization of several response variables *J. Qual. Technol.* **12** 214–9
- [46] Senn T, Waberski C, Wolf J, Esquivel J P, Sabate N and Lochel B 2011 3D structuring of polymer parts using thermoforming processes *Microelectron. Eng.* **88** 11–6
- [47] Xia Y N, Kim E, Zhao X M, Rogers J A, Prentiss M and Whitesides G M 1996 Complex optical surfaces formed by replica molding against elastomeric masters *Science* **273** 347–9